

High redshift radio quiet quasars – exploring parameter space of accretion models. Part II: patchy corona model

Małgorzata A. Sobolewska

Harvard-Smithsonian Center for Astrophysics, 60 Garden Street, Cambridge, MA 02138
Nicolaus Copernicus Astronomical Center, Bartycka 18, 00-716 Warszawa, Poland

msobolewska@cfa.harvard.edu, malsob@camk.edu.pl

Aneta Siemiginowska

Harvard-Smithsonian Center for Astrophysics, 60 Garden Street, Cambridge, MA 02138

asiemiginowska@cfa.harvard.edu

and

Piotr T. Życki

Nicolaus Copernicus Astronomical Center, Bartycka 18, 00-716 Warszawa, Poland

ptz@camk.edu.pl

ABSTRACT

We modeled the spectral energy distribution (SED) of high redshift radio quiet quasars (high- z RQQs). We computed spectra in a patchy corona geometry where an accretion disk extends to the last stable orbit and the Comptonizing active regions (hot clouds) are distributed above the disk. We explored the model parameter space to find theoretical parameters that give spectra with the optical/UV luminosity, the X-ray loudness, and the X-ray photon index compatible with those of high- z RQQs observed with *Chandra*. We found that a range of solutions is possible, from high- kT_e low- τ to low- kT_e high- τ models. The solutions require low level of energy dissipation in the hot clouds and low disk covering factor. The modeled mass is of the order of $10^{10} M_\odot$ and the accretion rate is $\dot{M} \geq 0.2 \dot{M}_{\text{Edd}}$. We compare our results to those obtained previously for hot inner flow geometry.

Subject headings: accretion, accretion disks — galaxies: high-redshift — quasars: general — X-Rays

1. Introduction

Modeling quasars’ broad band energy spectra provides important information about the geometry and environment of the quasars at different epochs. Such spectra are thought to originate in an accretion of matter onto a massive black hole (Rees 1984). In the standard scenario a thin accretion disk that is formed thermalizes the gravitational potential energy and radiates it as a disk black body giving a characteristic bump in the spectrum (Shakura & Sunyaev 1973). In the case of high redshift quasars, this bump is shifted into the optical/UV range (Shields 1978), which makes it easy to observe and study. The X-ray part of the spectrum is believed to originate in an inverse Compton process of the disk photons on energetic electrons. Modeling the X-ray component gives a direct information about the geometry of the accretion flow (i.e. the relative location of the cold accretion disk and Comptonizing plasma). Radio quiet quasars are good objects for such studies since their X-ray spectra are not “contaminated” by any additional components connected to the radio emission. Moreover, the radio quiet quasars comprise majority among the quasars population (Stern et al. 2000). They are more common, and hence more typical. Recent X-ray observations of quasars located at redshift $z > 4$ (e.g. Becker et al. 2001; Brandt et al. 2002a; Bechtold et al. 2003, hereafter B03) provide for the first time a unique opportunity to study these objects at the early Universe and investigate their evolution. Thus, we focus our study on the high redshift radio quiet quasars (high- z RQQs).

The observations of accreting sources support the hypothesis that the accretion flow is composed of a cold medium producing a thermal radiation and a hot medium radiating in X-rays. The puzzling question is that of a relative location of these two phases. A variety of geometries has been considered in order to explain the observed spectra and correlations. In Sobolewska, Siemiginowska & Życki 2004 (hereafter Paper I) we shortly reviewed currently considered scenarios for the accretion flow which were successful in explaining spectra of galactic X-ray binaries (XRB) and Seyfert galaxies. We discussed possible tests of geometry that can be conducted based on modeling the broad band spectra. In particular, a correlation between the amplitude of reflection, R , and the X-ray photon index, Γ , observed in X-ray binaries and Seyfert galaxies (Zdziarski, Lubiński, & Smith 1999) seems to be one of the criteria. Such correlations can be reproduced by the following models: (1) a truncated disk surrounding a hot inner flow (Zdziarski et al. 1999), (2) a hot corona formed by active regions above the disk, outflowing at relativistic speeds (Beloborodov 1999a, hereafter B99), (3) a cold disk covered by a hot ionized skin which decreases the effectiveness of thermalization (Nayakshin, Kazanas & Kallman 2000) (4) a hot spherical inner flow surrounded by cold clouds (Malzac 2001). In Paper I we investigated in details the first possibility. We assumed that the accretion flow in high- z RQQs proceeds through a standard optically thick cold accretion disk covered with a hot corona. At a certain radius the disk was assumed to

evaporate and a hot inner flow was formed. We computed spectra in such geometry and explored the model parameter space. We found that modeling both the optical/UV and X-ray component provides tight constraints on the Comptonizing plasma parameters through the observed X-ray loudness parameter, α_{ox} , X-ray photon index, Γ , and the optical/UV luminosity, $l_{\text{UV}} \equiv \log(\nu L_\nu)$ at $\nu = c/\lambda_{2500\text{\AA}}$ in the rest frame. For most objects the truncation radius is required to be larger than the radius of the innermost stable orbit, $r_{\text{tr}} > 3 R_{\text{S}}$, with an upper limit of $r_{\text{tr}} \leq 40 R_{\text{S}}$ (where $R_{\text{S}} = \frac{2GM}{c^2}$ is a Schwarzschild radius). We also concluded that the advection in the inner hot flow may play an important role. Moreover, the shape of the inner hot flow may deviate from spherical one. Instead, it may be considerably flattened. Our modeling suggested high accretion rates, $\dot{M} \geq 20\% \dot{M}_{\text{Edd}}$ which may suggest similarity of high- z RQQs to XRBs in the high state (HS) or very high state (VHS) of black hole X-ray binaries. However, in these spectral states the accretion disk is thought to extend to the last stable orbit. This provides motivation for investigating the geometry of a disk extending to the innermost stable orbit, with some kind of an X-ray active corona.

In this paper we investigate such an active corona geometry. The structure of the paper is as follows. In Section 2 we describe the model. In Section 3. we present the results. Section 4. contains application of the model to the sample of high- z quasars from B03. Finally, in Section 5. we discuss the results and give the concluding remarks.

2. Model

The plane-parallel geometry in which the accretion disk extends to the innermost circular orbit and the hot corona is located above the disk does not reproduce the photon index less than ~ 2 (Haardt & Maraschi 1991, Stern et al. 1995). According to Vignali et al. (2003a, hereafter V03) the mean X-ray photon index of high- z radio quiet quasars is $\Gamma \sim 2$, so the model in which this value is somehow limiting does not seem to offer enough flexibility in explaining the distribution of photon indices around the derived mean. Moreover, the mean X-ray photon index from the sample of B03 is ~ 1.5 . The plane parallel geometry can be modified in order to account for harder spectra. Here, we consider a case in which the hot Comptonizing plasma is not continuous but is composed of a number of active regions distributed above the accretion disk (driven by, e.g., magnetic reconnection events; Galeev, Rosner, & Vaiana 1979; Haardt, Maraschi, & Ghisellini 1994; B99; Malzac, Beloborodov, & Poutanen 2001). The geometry is schematically presented in Figure 1. Additionally, the hot plasma can move toward to or away from the disk (B99).

We assume that the innermost stable orbit is located at $r_{\text{in}} = 3 R_{\text{S}}$, and the accretion efficiency is $\epsilon = 1/12$.

The computed spectra are a sum of a Comptonized component and thermal disk radiation that escapes the hot plasma without being scattered or does not encounter the hot plasma on its way to the observer.

2.1. The Comptonized component

We consider a thermal Comptonization case, i.e. we assume that the Comptonizing electrons have purely thermal (Maxwellian) energy distribution. We compute the Comptonized component using the EQPAIR code of P. Coppi, described in detail in, e.g., Coppi (1999). The main parameters of the code are the plasma heating rate, l_h , and the soft photon compactness, l_s ($l \equiv (L/R)\sigma_T/(m_e c^3)$, where L is the luminosity and R is the size of the plasma cloud). In addition, we need to specify the spectrum of input soft photons, and background plasma optical depth, τ_p . The code includes all relevant microphysical processes of interactions between plasma and radiation. It computes plasma parameters: the temperature, kT_e and total optical depth, including the contribution from electron-positron pairs, as well as the spectrum of Comptonized emission.

In practice we parameterize our results by the ratio l_h/l_s , and the plasma temperature, kT_e . The former is convenient since it is easily computed from an assumed geometry (see below), and it is the most important parameter to determine the spectral slope of radiation (e.g. Beloborodov 1999b). The temperature replaces the heating compactness, l_h , which is more difficult to estimate observationally. To achieve the required value of kT_e one should iterate the computations over the total optical depth. In practice, we iterate over l_h for a pure pair plasma (see also Haardt & Maraschi 1991). We consider the low- and high-temperature regimes ($kT_e = 100$ and 300 keV, respectively), since there are no observational data to constrain this parameter in the case of high- z RQQs. The spectrum of soft input photons is the disk blackbody spectrum constructed as described below in Sec. 2.2.

The ratio l_h/l_s (or equivalently the amplification factor, A , $l_h/l_s \equiv A - 1$) can be computed from the geometrical parameters describing the plasma clouds: μ_s defined in eq. 5, the disk covering factor, C , and the fraction of energy dissipated in the corona, f . We write

$$A = \frac{L_{\text{soft}} + L_{\text{diss}}}{L_{\text{soft}}}, \quad (1)$$

where L_{diss} is the dissipation rate of gravitational energy in the corona (the clouds), and L_{soft} is the luminosity of the disk radiation cooling the hot plasma.

We follow the calculations of B99, but we assume that only a fraction of the available gravitational energy, $f \leq 1$, is dissipated by the clouds above the disk. The luminosity of

the hot clouds is thus

$$L_{\text{diss}} = f\epsilon\dot{M}c^2. \quad (2)$$

If the emitting plasma moves with high velocity, the luminosity transforms from the source (plasma) frame to the observers frame with δ^3 , where $\delta = [\gamma(1 - \beta\mu)]^{-1}$ is a Doppler factor (Rybicki & Lightman 1979), and $\mu = \cos\theta$, $\gamma^2 = 1/(1 - \beta^2)$, $\beta = v/c$ is the vertical velocity of the clouds (negative β means movement toward the disk). Also, $\int_{-1}^1 L_{\text{diss}}(\mu)d\mu = L_{\text{diss}}$, where $L_{\text{diss}}(\mu)$ is the angular distribution of the clouds luminosity in the observer frame. Therefore,

$$L_{\text{diss}}(\mu) = \frac{f\epsilon\dot{M}c^2}{2\gamma^4(1 - \beta\mu)^3}. \quad (3)$$

The hard radiation emitted by clouds illuminates the accretion disk. A fraction $1 - a$ (a being the disk albedo) of it is thermalized in the disk, thus contributing to the disk emission. We use $a = 0.2$ as appropriate for relatively cold matter (Haardt & Maraschi 1993). As a result the total disk luminosity is:

$$L_{\text{disk}} = \epsilon\dot{M}c^2(1 - f) + (1 - a) \int_{-1}^0 L_{\text{diss}}(\mu)d\mu, \quad (4)$$

where the first term comes from the viscous dissipation in the disk, and the second one represents the contribution from the reprocessed radiation.

Not all the disk radiation cools the clouds, since only a fraction of the disk surface is covered by the clouds. We describe the fraction of the viscous disk radiation intercepted by the clouds by introducing the disk covering parameter, C . The fraction of the reprocessed radiation that returns to the clouds is parametrized by the cloud geometry factor, μ_s , defined as in B99 (see also Figure 1). The total luminosity that provides cooling of the clouds may be now written as:

$$L_{\text{soft}} = C(1 - f)\epsilon\dot{M}c^2 + (1 - a) \int_{-1}^{-\mu_s} L_{\text{diss}}(\mu)d\mu. \quad (5)$$

In such form, this equation allows for only a small fraction of the disk being covered by the clouds, opposite to what was done in Di Salvo et al. (2001), who assumed that the angular distribution of the viscous and reprocessed disk radiation is similar, i.e. the clouds must cover most of the disk's surface (cf. their equation (8)). In our approach, we expect $C \ll 1$ from the data modeling.

The amplification factor calculated in the plasma comoving frame (Rybicki & Lightman 1979; B99) takes the following form:

$$A = 1 + f \left[C(1 - f)\gamma^2 \left(1 - \frac{\beta(1 + \mu_s)}{2} \right) + \right.$$

$$+ (1 - a) \frac{f}{2\gamma^2} (1 - \mu_s) \frac{1 - \frac{\beta^2}{4}(1 + \mu_s)^2}{(1 + \beta)^2(1 + \beta\mu_s)^2} \Big]^{-1}, \quad (6)$$

which for $\beta = 0$ reduces to

$$A_{\beta=0} = 1 + \frac{f}{C(1 - f) + 0.5f(1 - a)(1 - \mu_s)} \quad (7)$$

Given the input disk spectrum (described below, Section 2.2), the Comptonization procedure computes the Comptonized component, and the component that escapes the clouds without being scattered.

2.2. The disk component

The disk spectrum is assumed to be a disk blackbody with the radial temperature profile of $T(r) = T_0 \left(\frac{r}{r_{\text{in}}}\right)^{-3/4} \left(1 - \sqrt{\frac{r_{\text{in}}}{r}}\right)^{1/4}$, where r is in Schwarzschild units. The constant T_0 is derived from the normalization condition that the total disk luminosity is L_{disk} . The disk photons that escape the system without encountering the clouds on their way have luminosity $L_{\text{esc}} = L_{\text{disk}} - L_{\text{soft}}$ (eq 4, 5).

The model is thus parametrized by:

- the mass of the black hole, M ,
- the accretion rate, $\dot{m} = \dot{M}/\dot{M}_{\text{Edd}}$,
- the fraction of gravitational energy released in the hot clouds, f ,
- the electron temperature, kT_e ,
- the geometry of the clouds, μ_s ,
- the disk covering factor, C , and
- the vertical velocity of the clouds, β .

3. Results

We compute the optical/UV/X-ray spectra based on the model described in the previous section. From the spectra we compute spectral characteristics such as the optical/UV luminosity, $l_{UV} \equiv \log(\nu L_\nu)$ at 2500 Å in the rest frame, the X-ray loudness, α_{ox} , the X-ray photon index, Γ , and compare them with observations. We explore the model parameters space to find theoretical parameters for which modeled spectra match the observational data best. In the high temperature case the X-ray spectrum deviates from the power-law-like shape due to the first scattering effects, and we compute the photon index as the index of the best power law fit to the model spectrum.

Below, we discuss in details the results with respect to the data of high-redshift RQQs. In particular we search for such values of the theoretical model parameters which give $\Gamma < 2.3$ and $1.5 < \alpha_{ox} < 1.8$. Such a choice is motivated by the 3σ confidence intervals of Γ given by V03 ($1.7 \leq \Gamma \leq 2.3$), results of Vignali et al. (2003c) ($\Gamma = 1.86_{-0.37}^{+0.41}$), and B03 sample with the mean photon index of $\Gamma = 1.50 \pm 0.15$ (the error represents the 90% confidence interval). We choose the value of $\alpha_{ox, \min} = 1.5$ for the lower limit motivated by the value within 3σ confidence interval found for RQQs in Bright Quasar Survey (see Brandt et al. 2002b and references therein). The upper limit of $\alpha_{ox, \max} = 1.8$ was chosen based on the samples of B03 with $\alpha_{ox} = 1.71 \pm 0.02$ (the contributions to the error of α_{ox} come only from errors of the X-ray photon index and the normalization of the power law fit to the data; also, the 2 keV flux in the source frame was calculated from the 1 keV flux in the observer frame assuming the photon indices found from fits, not the value of 2.2 as assumed in B03), and V03 with $\alpha_{ox} = 1.77 \pm 0.03$ (we cite the value of α_{ox} corrected by the authors in a subsequent paper, Vignali et al. 2003c).

First, we focus on the case with $\beta \equiv v/c = 0$, i.e. we assume that the clouds above the disk are static. Next, we check how the mildly relativistic motion of the clouds away from or towards to the accretion disk may affect the results.

Figure 3 shows the spectral changes due to the different model parameters. The fraction of energy dissipated in the hot clouds affects both the optical/UV luminosity and the X-ray slope (Fig. 3a). Variations of the accretion rate have almost no influence on α_{ox} and Γ (Fig. 3b), but the optical/UV luminosity is affected.

Variations of the plasma temperature affect the high energy cut-off of the X-ray continuum (Fig. 3f). In the spectra with high temperature (here computed for $kT_e = 300$ and 500 keV) the characteristic feature of the first scattering can be seen in model spectra. The models with low temperature (here $kT_e = 100$ and 150 keV) have the optical depth of the order of unity, while in case of high-temperature models the optical depth in the plasma is

significantly lower, which results in higher fraction of the radiation that escapes the plasma without scattering. In the case of significant coverage of the disk by the hot clouds this may result in noticeable variations in the X-ray loudness.

The rest frame ultraviolet luminosity, l_{UV} , depends only on the accretion rate, \dot{m} , the fraction of energy dissipated in the clouds, f , and the mass of the black hole, M . For the chosen mass ($M = 10^{10} M_{\odot}$), the observed in high- z RQQs l_{UV} is easily reproduced by any pair of f and \dot{m} . Hence, we focus only on investigating the range of the X-ray loudness, α_{ox} , and the X-ray slope, Γ , possible to obtain from the model.

The X-ray photon index does not depend on the accretion rate if all remaining parameters are fixed. This can be seen in Figure 3b. Also the X-ray loudness (in the interesting range, $\alpha_{ox} \sim 1.5 - 1.8$) does not depend significantly on the accretion rate for given cloud geometry, μ_s , fraction of energy dissipated in the cloud, f , and the disk covering factor, C . Hence, in this subsection we assume $\dot{M}=0.1 \dot{M}_{Edd}$.

For given f and C the X-ray spectra harden for higher cloud geometry parameter, μ_s , i.e. for the cloud that is more compact in the sense of horizontal dimension as seen from the disk. This effect is more pronounced for higher f (see Figure 3c). More compact clouds intercept less of their own reprocessed radiation. Less plasma cooling gives rise to hardening of the spectrum. If f is small, most of soft disk radiation comes from the viscous dissipation in the disk, and the amount of the soft photons for Comptonization in the cloud is determined by the disk covering parameter, C . High f means that in the soft disk flux the reprocessed hard cloud radiation dominates. Therefore, any change of cloud geometry affects the spectrum more in the high f case than in the low f case.

In Figure 4 we present the main results of our analysis. On the *disk covering factor - strength of the corona* plane, we indicate regions with $1.5 < \alpha_{ox} < 1.8$ and $1.7 < \Gamma < 2.3$. For horizontally extended clouds (with $\mu_s = 0.1$) it is not possible to obtain spectra with the photon index lower than approximately 2.2 (a). Figure (b) shows that for vertically extended clouds the region with the photon index of 1.7–2.0 appears in the parameter space.

Figure (c) illustrates the influence of the plasma temperature (the optical depth) on the parameter space. Increasing the electron temperature does not influence significantly the X-ray slope of the spectrum, which is determined by amplification factor, whose value follows from global energy balance (see, e.g., Beloborodov 1999ab). The X-ray loudness is mostly affected by the temperature changes in the region of $C > 0.1$.

Spectra with X-ray loudness of $\alpha_{ox} = 1.5-1.8$ are produced if the hot clouds dissipate $\sim 3-30\%$ of gravitational energy. The hardest and X-ray quietest spectra can be produced for the fraction of energy released in the clouds of 3–8%, and the disk covering factor of

$\leq 1\%$.

A mildly relativistic outflow of the plasma causes hardening of the spectra, whereas an inflow results in the softer X-ray photon index. This is due to the relativistic beaming of the radiation. We illustrate this effect in Figure 3e. Figure 4d shows the transformation of the solutions for α_{ox} and Γ in the case of outflow with velocity of $\beta \equiv v/c = 0.5$. Spectra with the photon index lower than ~ 1.7 can be obtained only assuming the outflowing corona. However, the quality of the data is not sufficient to draw the conclusions regarding the plasma velocity since there is no information about the reflected component. We discuss this problem further in the next Section.

4. Application to the data

We model spectra of all but two high redshift radio quiet quasars from the B03 sample. We omit two objects with the hardest spectra characterized by the X-ray photon index as low as ~ 0.3 – 0.7 . We do not perform a formal χ^2 fitting to determine the best-fit parameters and their confidence limits, but rather demonstrate the parameter values which approximately reproduce the spectra. With the available data the results are not unique, and a number of solutions is possible. The computed spectra are shown in Figures 5 and 6. The model parameters are listed in Tables 1 and 2. The objects were observed by *Chandra X-ray Observatory* and the data were filtered to include the 0.3–6.5 keV energy range. The 1450 Å rest frame points were taken from the literature, as described in details in B03. The ratio of the optical/UV and X-ray fluxes is characterized by the X-ray loudness. In the case of high- z quasars the 2500 Å flux used to calculate α_{ox} must be extrapolated from 1450 Å flux known from observations, which involves a knowledge of the optical/UV spectral index, α_{UV} ($f_\nu \sim \nu^{\alpha_{\text{UV}}}$). To derive general properties of a theoretical model or an observational sample, a mean value suggested by observations can be used (as in Section 3, or in B03 were $\alpha_{\text{UV}} = -0.3$ was adopted (Kuhn et al. 2001)). However, it does not apply to the spectral modeling of particular objects. Thus, in this section we use the flux at 1450 Å to normalize the spectrum, and we list values of the spectral index between rest frame 1450 Å and 2500 Å, α_{UV} , and the X-ray loudness, α_{ox} , computed from the model spectra in Tables 1 and 2. The optical and X-ray observations were not simultaneous. However, Giveon et al. (1999) argue that the optical variability anti-correlates with the luminosity of AGNs. Given that the high- z RQQs are very luminous objects, one would expect optical variability at a relatively small level.

Our modeling indicates that without information about the high energy cut-off a grid of solutions exists for every object. For each object we present fits to the spectra with kT_e

of 100 and 300 keV.

A method to distinguish between the low- kT_e high- τ and high- kT_e low- τ solutions could be obtained by high signal-to-noise data of the Comptonized continuum at ~ 0.1 – 10 keV band (in the source frame). High-temperature low- τ Comptonized continua show strong broad features from the first scattering, where the shape of the seed photon spectrum is imprinted in the Comptonized spectrum (e.g. Stern et al. 1995). We have to keep in mind though that the spectra are likely to be time variable and thus the observed continua correspond to time averaged parameters, which may not contain the specific features of a single temperature Comptonization.

From the modeling it follows that only less than 30% of the energy is dissipated in the corona.

The model is able to cover relatively wide range of α_{UV} parameter from -0.1 to -0.4 (see Tables 1 and 2). Knowing exact value of this spectral index for particular objects would provide yet another observable, which could help to determine the model parameters.

4.1. Static hot plasma clouds.

First we discuss the case with $\beta \equiv v/c = 0$, i.e. the hot clouds are static.

The data require a mass of the black hole of the order of $10^{10} M_\odot$. The accretion rate is rather high, $\dot{M} > 0.2 \dot{M}_{\text{Edd}}$. Certain degeneracy exists between the mass and the accretion rate (i.e. one can explain the data with either low masses and high accretion rates, or high masses and low accretion rates); see BRI0103+0032 in Table 1. In addition, the geometrical parameters are also connected. For example, we keep the strength of the corona constant and change the clouds geometry parameter, μ_s , between 0.9 and 0.8. To model the data in these two cases we need to adjust the disk covering factor, C . Alternatively, one can keep the disk covering factor constant, and adjust the strength of the corona. In this case, however, the X-ray loudness fixed by the data additionally requires the plasma to have lower optical depth.

To reproduce the observations the clouds need to be vertically elongated with $\mu_s > 0.4$, which to the first order corresponds to $H/R > 1$, where H is the height of the cloud and R is its radius (see Figure 2). The best fits presented in Figure 5 and 6 require $\mu_s = 0.8 - 0.9$, i.e. $H/R \sim 3 - 6$. For $\mu_s < 0.4$ the spectra are too soft. Increasing the strength of the corona, f , to harden the spectra results in wrong relative normalization of the X-ray and optical components.

The clouds intercept not more than $\sim 10\%$ of the viscous disk radiation: the covering factor is typically of the order of $10^{-4} - 10^{-3}$. This means that the clouds cover rather small fraction of the disk surface. Values of $C \ll 1$ are in agreement with our assumptions (see equation (5)). We perform also fits with $C = 0$ (which correspond to the case when the soft photons for Comptonization come solely from the reprocessed radiation) and the softest photon index allowed by the data to provide a lower limit for μ_s parameter.

In the case of the two objects with relatively soft X-ray spectra ($\Gamma > 2.3$, BRI1033-0327, and PSS1317+3531) the geometry of the clouds is very different. They can form horizontally extended clumps with $\mu_s < 0.5$. In addition, the configuration in which the corona covers the whole surface of the disk like in the standard plane-parallel geometry ($\mu_s = 0$, $C = 1$) is marginally possible in the low-temperature high-optical-depth case and can be realized in the high-temperature low-optical-depth case.

4.2. Moving hot plasma clouds

Now we consider a possibility that the clouds are moving with mildly relativistic velocities, outflowing for $\beta > 0$ (e.g. BRI0103+0032 in Table 1) and moving toward the disk for $\beta < 0$ (e.g. BRI1033-0327 in Table 1). However, the plasma velocity cannot be constrained by the present data because of insufficient number of observables, which results in degeneracies between the model parameters. It is not possible to uniquely determine the outflow velocity, β , and the clouds geometry parameter, μ_s , without information about the reflected component or the high energy cut-off (B99; see also Di Salvo et al. 2001). The amplitude of the reflected component does not depend on the clouds geometry (except for a possibility of the reflected photons to be destroyed while passing through the hot plasma). It is determined by the system inclination $\mu = \cos\theta$ and the clouds velocity (B99). The reflection amplitude is given by the following equation:

$$R_{\text{refl}} = \frac{(1 + \beta/2)(1 - \beta\mu)^3}{(1 + \beta)^2} \quad (8)$$

This problem is illustrated by the fits to BRI0103+0032 (Table 1). We decrease the clouds geometry parameter, μ_s , from 0.9 to 0.5 keeping $C = 0.0035$ constant. The only way to compensate for this change and obtain a spectrum with the same X-ray slope ($\Gamma = 1.88$) is to allow for an outflow with $\beta = 0.5$, and adjust the strength of the corona, f , to reproduce the correct relative normalization of X-rays and optical/UV emission. The two fits (with $\beta = 0$ and $\beta = 0.5$) are equally good with the present data.

The objects in the sample with X-ray spectra characterized by the photon index of

$\Gamma \leq 1.5$ can be modeled only assuming the outflow (with the exception of the quasar at $z = 6.28$ whose photon index has large uncertainty). We present fits with $\beta = 0.5$ explaining their spectra (see Figure 6 and Table 2).

5. Discussion

We have computed optical/UV/X-ray spectra from a two-component accretion flow in geometry with the hot clouds of plasma (e.g. a magnetically driven “active corona”) distributed above an accretion disk extending to the last stable orbit (Haardt et al. 1994; Stern et al. 1995). We assumed that the soft disk blackbody-like radiation was Comptonized in the hot plasma clouds, and the electron energy distribution in the hot plasma was thermal. We investigated a parameter space where the models can reproduce the observed spectra of high redshift radio quiet quasars, and we applied the models to the data of RQQs from the sample compiled by B03. The observed spectra can be characterized by three observables: (1) the luminosity at 2500 Å in the rest frame of the source, $l_{UV} \equiv \log \nu L_\nu \sim 46\text{--}47$, (2) the X-ray loudness, $\alpha_{ox} \sim 1.5\text{--}1.8$, (3) the X-ray photon index, $\Gamma \sim 1.7\text{--}2.3$. These parameters imply that, for most of objects from the sample, the spectra are dominated by the disk thermal component, but the hard X-ray continua are rather hard.

Modeling the spectra we found that the angular size of the Comptonizing clouds as seen from the accretion disk should be small, $\mu_s \equiv \cos \theta \sim 0.8\text{--}0.9$ for best fit models, which corresponds to the ratio of height to radius $H/R \sim 3\text{--}6$ (Fig. 1). The clouds dissipate up to $\sim 30\%$ of gravitational energy, and intercept less than $\sim 10\%$ of viscous disk radiation.

In Paper I (the case of hot inner flow geometry) we have found that the plasma seems to have rather low optical depth (high electron temperature). Here we also find this kind of solution (with kT_e of 300 keV and $\tau \sim 0.02\text{--}0.5$) possible. However, the modeling is not unique because of too small number of observables. For each object a grid of models exists parameterized by, for example, plasma temperature. Solutions with low plasma temperatures and optical depths ~ 1 are possible, and these parameters are comparable to those of Seyfert galaxies and XRBs (although the broad band spectra are rather different, see below). These solutions however require very low energy dissipation in the hot clouds and small disk covering factor.

Possible bulk outflow velocity of the plasma (B99) is not constrained by the present data of high- z RQQs because of the lack of information about the reflected component. Malzac et al. (2001) discuss effects of scattering and attenuation of the reflected component traveling through the active region in patchy corona geometry, which may affect the equation (8).

They assumed cylindrical shape of active coronal regions, which results in different numerical coefficients in $\Gamma(A)$ dependence (see Beloborodov 1999b) than in the case of spherical clouds, but the overall trends should be similar. They concluded that these effects are strong for small H/R ratios (which corresponds to small μ_s) reducing the amount of reflection, and negligible for high H/R ratios (high μ_s). In the static case they obtained hard spectra and $R_{\text{refl}} = 1$ for high H/R , and soft spectra and $R_{\text{refl}} < 1$ for small H/R . Thus, the static patchy corona produces $R_{\text{refl}} - \Gamma$ anticorrelation instead of the observed correlation for X-ray Binaries and Seyferts (Zdziarski et al. 1999). The correlation can be obtained if we consider a possibility of the clouds outflow/inflow in the model. There exist no data for high- z RQQs to check whether the $R_{\text{refl}} - \Gamma$ correlation holds also for these objects.

The two models considered in this paper and Paper I give similar estimates on the mass of the black hole in high- z RQQs. The required mass is of the order of $(0.5\text{--}1.5) \times 10^{10} M_{\odot}$. The predictions on the fraction of energy dissipated in the hot plasma above the disk are slightly different. The patchy corona model allows for as much as $\sim 30\%$ of the dissipation to take place in the hot plasma, whereas in the model with truncated disk and hot inner flow as described in Paper I only about 10% of the energy may be dissipated in the corona above the disk (unless the spectra are soft, with $\Gamma > 2.3$). The accretion rates are comparable in both models, $\dot{M} > 0.20 \dot{M}_{\text{Edd}}$.

Spectra of objects in our sample are rather different from spectra of local Seyfert galaxies. The quasars spectra are strongly disk-dominated, yet the X-ray continua can be extremely hard. There is also greater variety of hard X-ray spectral slopes, despite relatively narrow range of mass accretion rate. In local Seyfert 1 galaxies the disk component appears to carry comparable luminosity as the hard X-ray component (e.g. NGC 5548, Chiang & Blaes 2003; MCG-6-30-15, Reynolds et al. 1997), while the X-ray slope is in the range 1.7–2. On the other hand, spectra of Narrow Line Seyfert 1 galaxies, thought to accrete at rather high \dot{m} , are disk dominated (e.g. Puchnarewicz et al. 2001), but their X-ray continua are rather soft, $\Gamma > 2$ (Brandt et al. 1997; Leighly 1999; Janiuk, Czerny & Madejski 2001).

Even more interesting is the comparison of the distant quasars with black hole binary systems in their high \dot{m} spectral states (High State and Very High State, see review by Done 2002). In these states the ratio of fluxes in the hard Comptonized and disk components can be anywhere between ≈ 0 and ≈ 1 , but the hard X-ray slope is $\Gamma \geq 2$ (e.g. Done & Gierliński 2003). Such strongly disk-dominated spectra with very hard Comptonized continua are rarely observed. This has prompted Gierliński & Done (2004) to propose that the spectra of quasars are strongly affected by photo-absorption. The intrinsic spectra would be similar to black hole binaries in (Very) High State, but strong absorption, possibly from a wind, results in apparent hard continua, with an apparent strong soft X-ray excesses. Obviously, if

their idea is correct, the parameters of an active corona would be completely different from what we have determined. In particular, the high energy X-ray continuum in XRB is usually explained as nonthermal Comptonization, since it is observed up to ~ 1 MeV without any significant spectral breaks (Grove et al. 1998).

Vignali et al. (2003b) report on the observed anti-correlation between the X-ray loudness (defined in their paper as negative) and the optical/UV luminosity in high- z RQQs. In Paper I and in the present paper we defined the X-ray loudness as positive. Below we discuss qualitatively, how the correlation can be obtained within the framework of the two geometries, the hot inner flow (Paper I) and the patchy corona (this paper).

In the model studied in Paper I (the truncated disk with the hot inner flow), changes of the disk truncation radius provide a natural qualitative explanation for this correlation. If the disk truncation radius becomes smaller (i.e. the inner edge of the disk moves towards the last stable orbit) the optical/UV luminosity rises. Also, the X-ray spectrum becomes softer which causes a drop in the 2 keV rest frame flux. Both higher optical/UV luminosity and lower 2 keV rest frame flux cause a rise in the X-ray loudness. As a result a correlation between optical/UV and the X-ray loudness can be obtained in the model. The other model parameters that influence the optical/UV luminosity are the accretion rate and the strength of the corona. However, in the hot inner flow model the corona above the disk is required to be weak with $f \leq 10\%$, and the accretion rate only slightly influences the X-ray loudness, so their impact on the observed correlation less significant than the change in the truncation radius.

In the patchy corona geometry (this paper) variations in the strength of the corona formed by hot clouds can account for the correlation between the X-ray loudness and optical/UV luminosity. If smaller fraction of gravitational energy is dissipated in the clouds, the disk thermal radiation is stronger and the optical/UV luminosity rises. At the same time the X-ray spectrum becomes softer. Thus the $\alpha_{\text{ox}} - l_{\text{UV}}$ correlation can be obtained. Fluctuations of the clouds geometry parameter, μ_s and the accretion rate, \dot{m} , also affect the optical/UV luminosity. However, based on our modeling of the quasars' data a narrow range of μ_s (0.8–0.9) is required, and in addition the X-ray loudness does not vary significantly with \dot{m} . Thus the energy dissipation in the corona could be the main driver for $\alpha_{\text{ox}} - l_{\text{UV}}$ correlation in this model.

We note that the observed value of the X-ray loudness depends on the assumptions concerning the optical/UV spectral index and the X-ray slope. The optical/UV spectra are affected by the intrinsic reddening which is usually unknown, so the UV spectral index has large uncertainties. Kuhn et al (2001) provides the best to date high redshift quasars optical/UV spectra and their value of $\alpha_{\text{UV}}=-0.3$ is different from the mean value of the Sloan

Digital Sky Survey quasars sample of -0.79 ± 0.34 (Fan et al 2001). Brandt et al. (2002a) analyzed X-ray spectra of the three highest redshift quasars known ($z = 6.28, 5.99, 5.82$) assuming the average value for the photon index derived by V03 ($\Gamma \sim 2$) and $\alpha_{UV} = -0.5$ (see references in Brandt et al. 2002a). They obtained $\alpha_{ox} \sim 1.68, 1.60, 1.58$, respectively. B03 used $\Gamma = 2.2$ (Laor et al. 1997) and $\alpha_{UV} = -0.3$ (Kuhn et al. 2001) for the same objects and obtained $\alpha_{ox} \sim 1.61, 1.54, 1.55$, respectively. We used the photon indices provided by B03 based on the spectral fit to the *Chandra* data. Our spectral model applied to these quasars gave spectra with the X-ray loudness of 1.78–1.79, 1.69, and 1.66–1.70, respectively (Tables 1 and 2). As shown in this paper and in Paper I, the α_{ox} parameter is one of the most important observables for high- z RQQs and it is important to understand its dependence on Γ and α_{UV} .

Obviously, tighter constraints on model parameters could be obtained with larger number of observables. The most promising at the present is the usage of optical/UV data for better modeling the optical/UV spectral index. This would allow to constrain better the mass and the accretion rate in the models. Another diagnostic would be measurements of the amount of reflection which could discriminate between uniform and non-uniform corona, or truncated accretion disk scenario. In addition, the observations of the amount of broadening of the iron $K\alpha$ line can provide estimates on the truncation radius. The observation of the high energy cut-off in the hard X-ray data would dramatically improve our understanding on the high- z RQQs spectra. However, the two latter tests require good quality data at least up to 30 keV in the rest frame, which might be possible with the future missions such as Constellation-X or NuSTAR for example.

6. Conclusions

In this paper we applied the patchy corona model to high- z RQQs, and explored the model parameter space. We compared the results to the results of the truncated disk with the hot inner flow model studied in Paper I. Our results show that:

1. If the hard X-ray part of the observed high- z RQQs spectra originates in the Comptonization process in the corona formed by hot clouds above an accretion disk, the clouds must be vertically elongated and intercept less than $\sim 10\%$ of the accretion disk radiation.
2. Similarly as in the hot inner flow model, the observed X-ray loudness and the photon index put strong constraints on the modeled optical depth. However, the number of observables is too small to uniquely determine the Comptonizing plasma parameters, and the grid of solutions with different pair (τ, kT_e) is possible for each object.

3. Both models require a similar mass of the black hole (of the order of $10^{10} M_{\odot}$), and accretion rates ($\dot{M} > 0.2 \dot{M}_{\text{Edd}}$).
4. In the patchy corona model a higher fraction of energy is allowed to be dissipated in the hot plasma above the disk than in the hot inner flow model.
5. The objects in the sample with X-ray spectra characterized by the photon index of $\Gamma \leq 1.5$ can be modeled only assuming the outflowing corona.
6. Future high quality observational data, both in the optical/UV and X-rays can significantly improve constraints on the model parameters and help to discriminate between different accretion flow geometries.

We thank our referee for careful reading of the manuscript. This research is funded in part by NASA contract NAS8-39073. Partial support for this work was provided by the National Aeronautics and Space Administration through Chandra Award Number GO1-2117B and GO2-3148A issued by the Chandra X-Ray Observatory Center, which is operated by the Smithsonian Astrophysical Observatory for and on behalf of NASA under contract NAS8-39073. MS and PTZ were partially supported by PBZ-KBN-054/P03/2001, and KBN projects number 2P03D00322, 2P03D01225. MS acknowledges support from the Smithsonian Institution Pre-doctoral fellowship program.

REFERENCES

- Bechtold, J. et al. 2003, ApJ, 588, 119 (B03)
- Becker, R. H. et al. 2001, AJ, 122, 2850
- Beloborodov, A. M. 1999a, ApJ, 510, L123 (B99)
- Beloborodov, A. M. 1999b, ASP Conf. Ser. 161: High Energy Processes in Accreting Black Holes, 295
- Brandt, W. N. et al. 2002a, ApJ, 569, L5
- Brandt, W. N. et al. 2002b, astro-ph/0212082
- Brandt, W. N., Mathur, S., & Elvis, M. 1997, MNRAS, 285, L25
- Chiang, J. & Blaes, O. 2003, ApJ, 586, 97
- Coppi, P. S. 1999, ASP Conf. Ser. 161: High Energy Processes in Accreting Black Holes, 375

- Di Salvo, T., Done, C., Życki, P. T., Burderi, L., & Robba, N. R. 2001, *ApJ*, 547, 1024
- Done, C. 2002, *Royal Society of London Philosophical Transactions Series A*, 360, 1967
- Done, C. & Gierliński, M. 2003, *MNRAS*, 342, 1041
- Fan, X. et al. 2001, *AJ*, 121, 54
- Galeev, A. A., Rosner, R., & Vaiana, G. S. 1979, *ApJ*, 229, 318
- Gierliński, M. & Done, C. 2004, *MNRAS*, 349, L7
- Giveon, U., Maoz, D., Kaspi, S., Netzer, H., & Smith, P. S. 1999, *MNRAS*, 306, 637
- Grove, J. E., Johnson, W. N., Kroeger, R. A., McNaron-Brown, K., Skibo, J. G., & Philips, B. F. 1998, *ApJ*, 500, 899
- Haardt, F. & Maraschi, L. 1993, *ApJ*, 413, 507
- Haardt, F. & Maraschi, L. 1991, *ApJ*, 380, L51
- Haardt, F., Maraschi, L., & Ghisellini, G. 1994, *ApJ*, 432, L95
- Janiuk, A., Czerny, B., & Madejski, G. M. 2001, 557, 408
- Kuhn, O., Elvis, M., Bechtold, J., & Elston, R. 2001, *ApJS*, 136, 225
- Laor, A., Fiore, F., Elvis, M., Wilkes, B. J., & McDowell, J. C. 1997, *ApJ*, 477, 93
- Leighly, K. M. 1999, *ApJS*, 125, 317
- Malzac, J., Beloborodov, A. M., & Poutanen, J. 2001a, *MNRAS*, 326, 417
- Malzac, J. 2001b, *MNRAS*, 325, 1625
- Nayakshin, S., Kazanas, D., & Kallman, T. R. 2000b, *ApJ*, 537, 833
- Puchnarewicz, E. M., Mason, K. O., Siemiginowska, A., Fruscione, A., Comastri, A., Fiore, F., & Cagnoni, I. 2001, *ApJ*, 550, 644
- Rees, M. J. 1984, *ARA&A*, 22, 471
- Reynolds, C. S., Ward, M. J., Fabian, A. C., & Celotti, A. 1997, *MNRAS*, 291, 403
- Rybicki, G. B. & Lightman, A. P. 1979, *Radiative Processes in Astrophysics* (New York: Wiley)

- Shakura, N. I. & Sunyaev, R. A. 1973, *A&A*, 24, 337
- Shields, G. A. 1978, *Nature*, 272, 706
- Sobolewska, M. A., Siemiginowska, A., & Życki, P. T. 2004, *ApJ*, 608, 80 (Paper I)
- Stern, D., Djorgovski, S. G., Perley, R. A., de Carvalho, R. R., & Wall, J. V. 2000, *AJ*, 119, 1526
- Stern, B. E., Poutanen, J., Svensson, R., Sikora, M., & Begelman, M. C. 1995, *ApJ*, 449, L13
- Vignali, C., Brandt, W. N., Schneider, D. P., Garmire, G. P., & Kaspi, S. 2003a, *AJ*, 125, 418 (V03)
- Vignali, C., Brandt, W. N., & Schneider, D. P. 2003b, *AJ*, 125, 433
- Vignali, C. et al. 2003c, *AJ*, 125, 2876
- Zdziarski, A. A. 1985, *ApJ*, 289, 514
- Zdziarski, A. A., Lubiński, P., & Smith, D. A. 1999, *MNRAS*, 303, L11

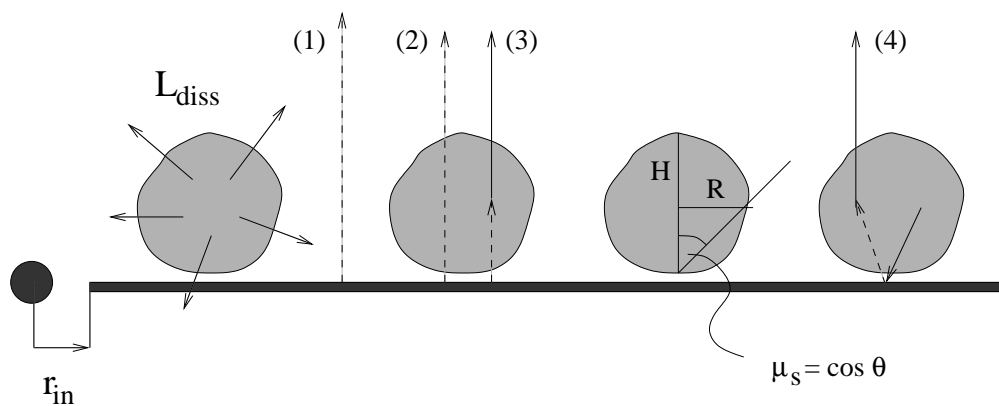


Fig. 1.— Patchy corona geometry. The accretion disk extends to the last stable orbit, r_{in} . The disk is covered with a hot clouds whose total luminosity accounts for L_{diss} . The spectral components are: the disk blackbody-like radiation which escapes the system without encountering hot plasma (1) or without being scattered in the hot plasma (2), and Comptonized component. The soft photons for Comptonization come from viscous dissipation in the disk (3) or reprocessing of the hot plasma radiation (4). The interpretation of the clouds geometry parameter, μ_s , is illustrated. See also Figure 2.

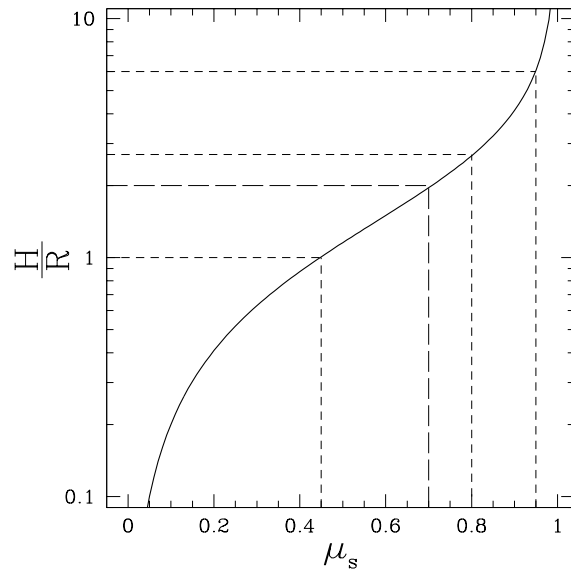


Fig. 2.— Interpretation of the clouds geometry parameter, μ_s . H denotes the height of the cloud, and R denotes the cloud radius. The clouds are approximately spherical for $H/R \sim 2$, which corresponds to $\mu_s \sim 0.7$. For $\mu_s \sim 0.8 - 0.95$ the clouds are vertically extended with $H/R \sim 3-6$. The height and radius of the clouds are of the same order for $\mu_s \sim 0.45$. The plane-parallel geometry corresponds to the case with $\mu_s = 0$.

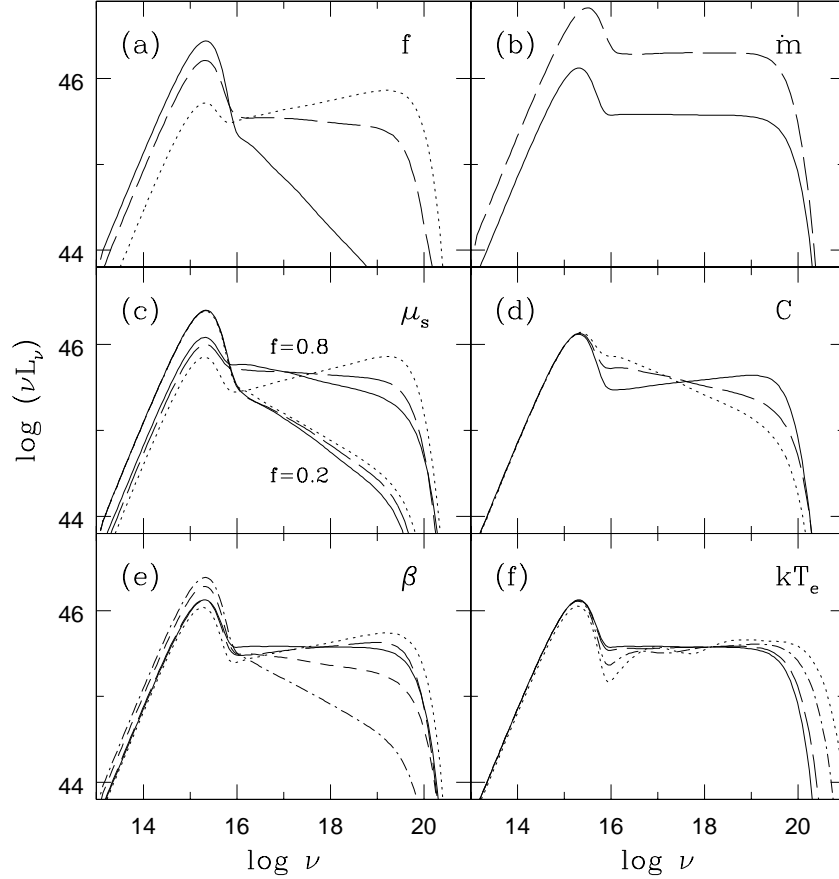


Fig. 3.— Dependence of spectra on the model parameters. Unless stated differently, the fixed parameters are: $M = 10^{10} M_{\odot}$, $\dot{m} = 0.1$, $\mu_s = 0.8$, $C = 0.2$, $f = 0.6$, $\beta = 0$, $kT_e = 100$ keV; (a) the fraction of energy dissipated in the corona, $f = 0.1$ (*solid curve*), 0.5 (*long-dashed curve*), 0.9 (*dotted curve*); (b) the accretion rate in Eddington units, $\dot{m} = 0.1$ (*solid curve*), 0.5 (*long-dashed curve*); (c) the cloud geometry parameter, $\mu_s = 0.1$ (*solid curve*), 0.5 (*long-dashed curve*), 0.9 (*dotted curve*); (d) the disk covering factor, $C = 0.1$ (*solid curve*), 0.5 (*long-dashed curve*), 0.9 (*dotted curve*); (e) the vertical velocity of the clouds, $\beta = -0.5$ (*dashed curve*), -0.2 (*dot-dashed curve*), 0 (*solid curve*), 0.2 (*long-dashed curve*), 0.5 (*dotted curve*); (f) the electron temperature, $kT_e = 100$ (*solid curve*), 150 (*long-dashed curve*), 300 (*dot-dashed curve*), 500 (*dotted curve*) keV.

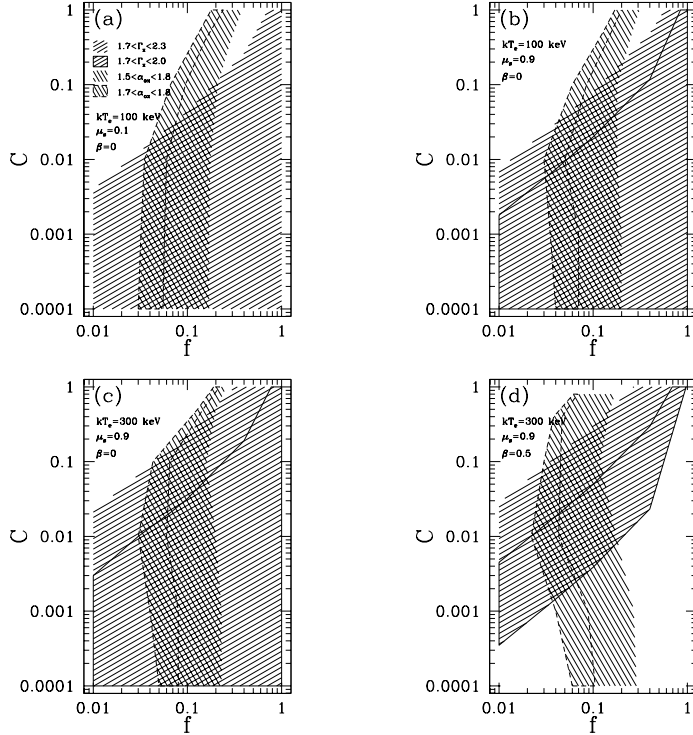


Fig. 4.— Overlapping of regions with $1.5 < \alpha_{\text{ox}} < 1.8$ and $1.7 < \Gamma < 2.3$ in the plane of the disk covering factor, C , and the fraction of energy dissipated in the clouds, f . The computations were done for (a) $\mu_s=0.1$, $kT_e = 100$ keV, $\beta = 0$, (b) $\mu_s = 0.9$, $kT_e = 100$ keV, $\beta = 0$, (c) $\mu_s = 0.9$, $kT_e = 300$ keV, $\beta = 0$, (d) $\mu_s = 0.9$, $kT_e = 300$ keV, $\beta = 0.5$. The fixed parameters are $M = 10^{10} M_{\odot}$, $\dot{M} = 0.1 \dot{M}_{\text{Edd}}$. Extended clouds ($\mu_s = 0.1$) produce spectra with $\Gamma \geq 2$ (a). In order to obtain spectra with $\Gamma = 1.7-2$ the clouds should be compact (b,c) and/or move away from the disk (d).

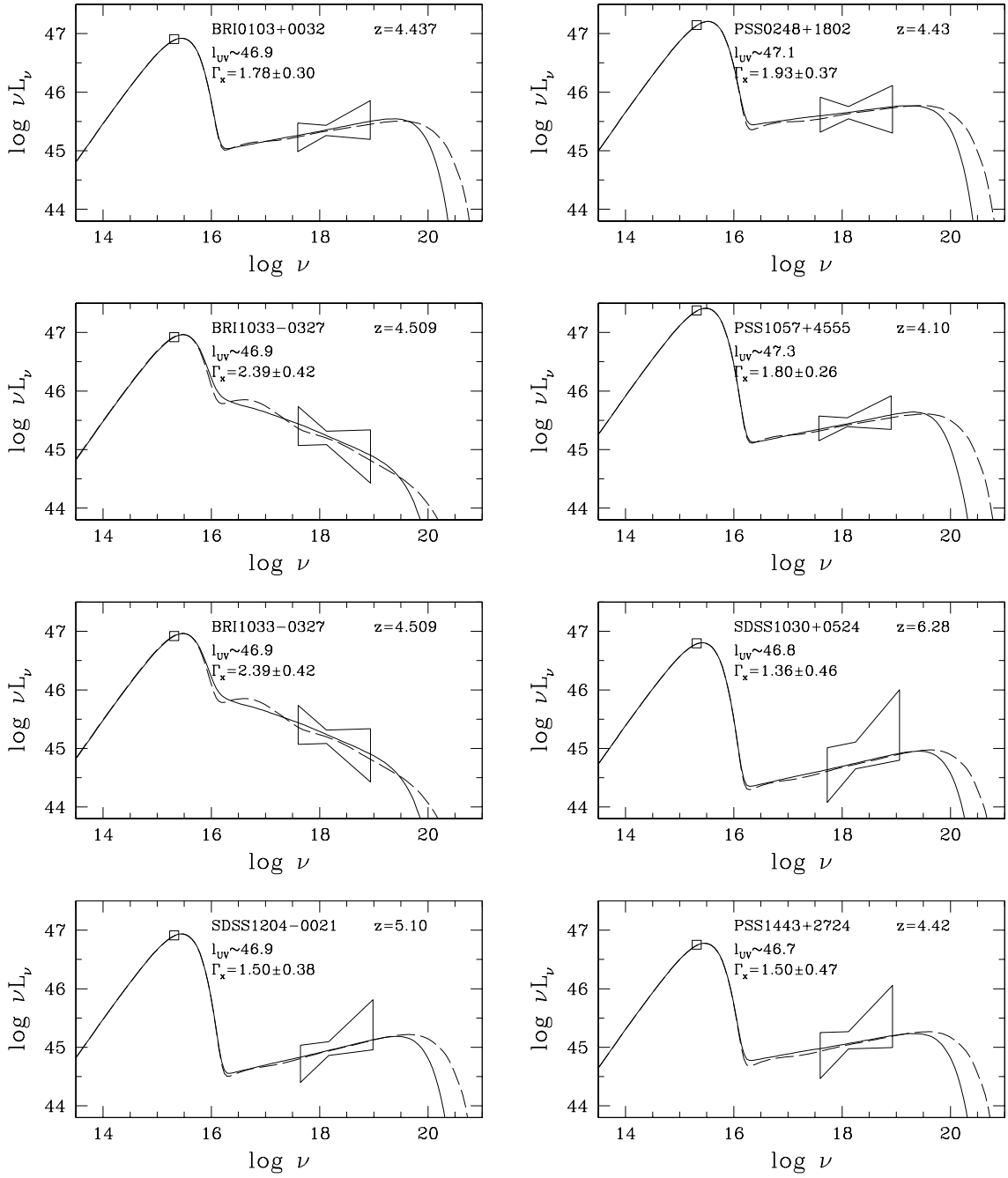


Fig. 5.— Modeling the objects from the B03 sample in the static clouds case ($\beta = 0$) for $kT_e = 100$ keV (*solid curve*), 300 keV (*dashed curve*). The parameters of the fits are listed in Table 1.

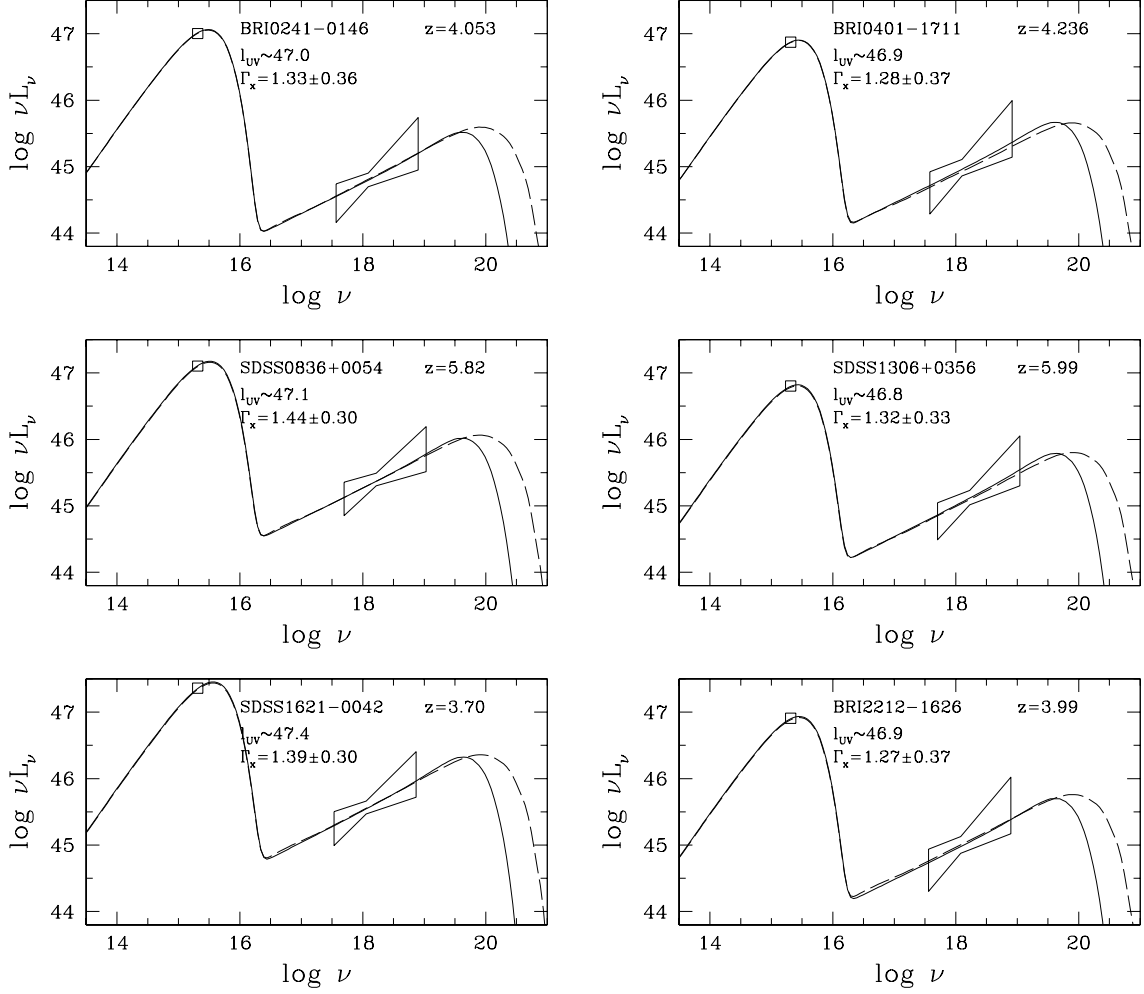


Fig. 6.— Modeling the objects from the B03 sample in the outflowing corona case ($\beta = 0.5$) for $kT_e = 100$ keV (*solid curve*) and 300 keV (*dashed curve*). The parameters of the fits are listed in Table 2.

Table 1. Modeling the SED of high- z RQQs.

OBJECT	m^a	\dot{m}^b	f^c	μ_s^d	C^e	β^f	kT_e^g	τ^h	Γ_{fit}^i	α_{UV}^i	α_{ox}^i
BRI0103+0032	1×10^{10}	0.31	0.11	0.9	0.004	0	100	0.91	1.82	-0.35	1.56
	1×10^{10}	0.31	0.11	0.9	0.0008	0	300	0.22	1.84	-0.35	1.57
	6×10^9	0.6	0.09	0.9	0.0035	0	100	0.91	1.82	-0.14	1.55
	6×10^9	0.6	0.1	0.8	0.0035	0	300	0.22	1.82	-0.15	1.54
	6×10^9	0.6	0.09	0.8	0.001	0	100	0.88	1.84	-0.14	1.54
	6×10^9	0.6	0.09	0.3	0	0	100	0.64	2.05	-0.14	1.51
	6×10^9	0.63	0.07	0.5	0.0035	0.5	100	0.91	1.82	-0.14	1.55
PSS0248+1802	1×10^{10}	0.6	0.11	0.8	0.004	0	100	0.81	1.88	-0.22	1.52
	1×10^{10}	0.60	0.11	0.8	0.006	0	300	0.20	1.85	-0.23	1.54
BRI1033-0327	1×10^{10}	0.35	0.15	0.5	0.15	0	100	0.36	2.40	-0.32	1.52
	1×10^{10}	0.35	0.13	0.1	0.35	0	300	0.04	2.30	-0.33	1.56
	1×10^{10}	0.43	0.3	0	1	0	100	0.20	2.78	-0.28	1.49
	1×10^{10}	0.4	0.153	0	1	0	300	0.02	2.45	-0.30	1.58
	1×10^{10}	0.36	0.2	0.8	0.15	-0.3	100	0.36	2.41	-0.31	1.52
PSS1057+4555	1.5×10^{10}	0.60	0.045	0.9	0.0015	0	100	0.9	1.82	-0.29	1.71
	1.5×10^{10}	0.60	0.047	0.9	0.0030	0	300	0.22	1.82	-0.29	1.72
	1.5×10^{10}	0.60	0.05	0.4	0	0	100	0.66	2.02	-0.29	1.66
PSS1317+3531	7×10^9	0.25	0.15	0.5	0.13	0	100	0.40	2.36	-0.32	1.52
	7×10^9	0.23	0.13	0.1	0.55	0	300	0.03	2.86	-0.34	1.47
	7×10^9	0.3	0.29	0	1	0	100	0.20	2.80	-0.28	1.51
	7×10^9	0.25	0.18	0	1	0	300	0.02	2.41	-0.33	1.55
SDSS1030+0524	1×10^{10}	0.22	0.037	0.9	0.0007	0	100	0.95	1.79	-0.42	1.78
	1×10^{10}	0.22	0.040	0.9	0.0010	0	300	0.25	1.78	-0.42	1.79
SDSS1204-0021	1×10^{10}	0.3	0.045	0.9	0.0007	0	100	0.96	1.78	-0.35	1.73
	1×10^{10}	0.2	0.050	0.9	0.001	0	300	0.27	1.77	-0.35	1.74
	1×10^{10}	0.3	0.045	0.8	0	0	100	0.88	1.84	-0.35	1.71
PSS1443+2724	8×10^9	0.27	0.08	0.9	0.0035	0	100	0.88	1.83	-0.33	1.61
	8×10^9	0.27	0.085	0.9	0.004	0	300	0.23	1.80	-0.33	1.63
	8×10^9	0.27	0.08	0.6	0	0	100	0.73	1.95	-0.33	1.59

^aBlack hole mass in Solar masses, M_{\odot}

^bAccretion rate in Eddington units, \dot{M}_{Edd}

^cFraction of gravitational energy dissipated in the clouds above the disk

^dCloud geometry parameter

^eDisk covering factor

^fVertical velocity of clouds

^gPlasma temperature in keV

^hPlasma optical depth

ⁱX-ray photon index allowed to vary within the 1σ confidence interval, the UV spectral index between 1450Å and 2500Å in the rest frame, and the X-ray loudness (we do not list l_{UV} from fits since its value was fixed at that observed)

Table 2. Modeling the SED of high- z RQQs.

OBJECT	m^a	\dot{m}^b	f^c	μ_s^d	C^e	β^f	kT_e^g	τ^h	Γ_{fit}^i	α_{UV}^i	α_{ox}^i
BRI0241-0146	1×10^{10}	0.4	0.025	0.9	0.0001	0.5	100	1.53	1.53	-0.29	1.86
	1×10^{10}	0.4	0.035	0.9	0.0001	0.5	300	0.51	1.52	-0.29	1.85
	1×10^{10}	0.4	0.023	0.85	0	0.5	100	1.53	1.53	-0.29	1.87
BRI0401-1711	1×10^{10}	0.29	0.05	0.9	0.0002	0.5	100	1.50	1.53	-0.36	1.75
	1×10^{10}	0.29	0.06	0.9	0.0003	0.5	300	0.48	1.55	-0.36	1.76
SDSS0836+0054	1×10^{10}	0.55	0.06	0.9	0.0003	0.5	100	1.52	1.53	-0.24	1.70
	1×10^{10}	0.55	0.08	0.9	0.0004	0.5	300	0.50	1.54	-0.24	1.69
	1×10^{10}	0.55	0.08	0.5	0	0.5	100	1.08	1.72	-0.24	1.66
SDSS1306+0356	1×10^{10}	0.25	0.075	0.9	0.0002	0.5	100	1.54	1.51	-0.40	1.69
	1×10^{10}	0.25	0.095	0.9	0.0003	0.5	300	0.51	1.53	-0.41	1.69
SDSS1621-0042	1.1×10^{10}	0.95	0.06	0.9	0.0002	0.5	100	1.58	1.51	-0.17	1.69
	1.1×10^{10}	0.95	0.08	0.9	0.0003	0.5	300	0.52	1.52	-0.17	1.68
BRI2212-1626	1×10^{10}	0.31	0.05	0.9	0.0002	0.5	100	1.51	1.53	-0.35	1.75
	1×10^{10}	0.31	0.07	0.9	0.0003	0.5	300	0.49	1.54	-0.35	1.73

^aBlack hole mass in Solar masses, M_{\odot}

^bAccretion rate in Eddington units, \dot{M}_{Edd}

^cFraction of gravitational energy dissipated in the clouds above the disk

^dCloud geometry parameter

^eDisk covering factor

^fVertical velocity of clouds

^gPlasma temperature in keV

^hPlasma optical depth

ⁱX-ray photon index allowed to vary within the 1σ confidence interval, the UV spectral index between 1450Å and 2500Å in the rest frame, and the X-ray loudness (we do not list l_{UV} from fits since its value was fixed at that observed)